ELSEVIER

Applied Surface Science 127–129 (1998) 184–192

applied surface science

A fast quantitative modelling of ns laser ablation based on non-stationary averaging technique

N. Arnold *, B. Luk'yanchuk, N. Bityurin

Angewandte Physik, Johannes-Kepler-University, A-4040 Linz, Austria

Abstract

A semi-analytical approach to a quantitative analysis of thermal ns laser ablation is presented. The nonlinear heat equation is reduced to three ordinary differential equations for the surface temperature, spatial width of the enthalpy distribution, and the ablated depth. Due to its speed and flexibility, the method provides a convenient tool for the fast analysis of experimental data. The influence of different factors on ablation curves (ablated depth h vs. fluence ϕ) is studied. Analytical formulas for threshold fluence ϕ_{th} and $h(\phi)$ dependences are discussed. The ablation curves reveal three regions of fluence: Arrhenius, linear, and the screening region. Small vaporization enthalpy results in a sub-linear but faster than logarithmic $h(\phi)$ dependence. Weakly-absorbing materials may exhibit two different ablation regimes – without or with ablation of the heated subsurface layer. The method is applied to the analysis of the single pulse ablation of polyimide. The single thermal evaporation energy ≈ 1.51 eV describes satisfactory the ablation at 248, 308 and 351 nm wavelengths.

PACS: 82.65; 82.50; 42.10; 81.15Fg

Keywords: Laser ablation; Thermal evaporation; Analytical modelling; Polymers

1. Introduction

Laser ablation is used in many technological applications [1]. One of the first questions to be clarified by the theoretical analysis is whether the experimental data can be explained by the thermal evaporation, or other mechanisms (photochemical bond breaking, hydrodynamics, non-equilibrium excitations, multi-photon or saturation processes) play an important role.

The present paper deals with *purely thermal surface* evaporation. There exists a gap between a simple analysis based on the linear heat equation, and numerical simulations with powerful computers. A feedback between the experimental and theoretical investigations requires a technique that permits rapid *quantitative* analysis of data on a PC. In the field of ns polymer ablation, the lack of quantitative analysis of experimental data on the basis of the purely thermal models lead to speculations and discussions [2]. For polymers, three quantities, absorption length, thermal length, and ablated depth, may be comparable in a typical experiment. Besides, activation temperature and enthalpy of vaporization may be significantly lower than for metals [3]. This makes the

* Corresponding author. Angewandte Physik, J.-Kepler-Universität, Altenbergerstraße 69, A-4040, Linz, Austria. Tel.: +43-732-2468-9243; fax: +43-732-2468-9242; e-mail: nikita.arnold@jk.uni-linz.ac.at.

0169-4332/98/$19.00
PII S0169-4332(97)00630-2

consideration of temperature dependences of specific heat and thermal conductivity more important [4], and at the same time, allows to avoid the consideration of the processes in the ionized plume.

We propose fast method to find an approximate solution to the *nonlinear* heat equation based on non-stationary averaging (e.g., Ref. [5]). It permits one to study the influence of: *temperature dependences* in specific heat, thermal conductivity, absorptivity; arbitrary *temporal profiles* of the laser pulse; strong dependence of the ablation velocity on the surface temperature; *screening* of the incoming radiation by the ablated products; ablation enthalpy; melting and/or other phase transformations. *Not included* are hydrodynamical effects, nonlinear optical effects, optical breakdown, and thermally induced stresses.

2. The model

For the analysis of thermal ablation, we use one-dimensional heat equation with ablation velocity $v = v(t)$ changing during the pulse [6]. We write it in terms of volumetric enthalpy $H(T) = \rho\int_{T_0}^{T} c(T_1)\mathrm{d}T_1$, where T is the temperature, c specific heat (per unit mass) of the condensed phase, and T_0 the ambient temperature. The density ρ is assumed to be constant. In the moving reference frame fixed with the ablation front [1]:

$$\frac{\partial H}{\partial t} = v\frac{\partial H}{\partial z} + \frac{\partial}{\partial z}\left(K(T)\frac{\partial T}{\partial z}\right) + I_s\alpha\exp(-\alpha z) \equiv B(z,t) \tag{2.1}$$

where K is the heat conductivity, and we introduced the notation B for the r.h.s. Latent heat of phase transformations can be included into $H(T)$. The intensity within the sample shall obey Bouguer equation. I_s is the intensity absorbed at the surface. Henceforth, index s will refer to the quantities at the surface $z = 0$. We adopt the following approximations. Following Refs. [7,8], we relate I_s to laser pulse intensity $I(t)$ by:

$$I_s = IA\exp\left[-\alpha_g h\right], \tag{2.2}$$

where A is the absorptivity, and α_g vapor absorption coefficient recalculated to the density of solid. Both may depend on T_s. The surface recession rate v shall be given by [1,7]:

$$v = v_0\exp(-T_a/T_s), \tag{2.3}$$

where T_a is the activation temperature. At $z = 0$, we assume *negative* thermal flux J_s [4,7]:

$$-K\frac{\partial T}{\partial z}|_{z=0} \equiv -D_s\frac{\partial H}{\partial z}|_{z=0} = -v\left[L + H_g(T_s) - H(T_s)\right] \overset{def}{\equiv} J_s. \tag{2.4}$$

$D_s \equiv K_s/\rho c_s$ is the thermal diffusivity, and the expression in square brackets is the enthalpy difference between the vapor and condensed phase at $T = T_s$. L is the volumetric latent heat of vaporization at $T_s = T_0$, $H_g(T) = \rho\int_{T_0}^{T} c_g(T_1)\mathrm{d}T_1$. c_g is the specific heat per unit mass of vapor. $T(z\to\infty)\to T_0$, and $T(t = 0) = T_0$.

This model is often applied for the description of laser ablation, and involves numerical solution of the *partial* differential equations. Below, we use the moments technique [5] to reduce it to three *ordinary* differential equations (ODE) which can be solved very fast by many computational packages.

3. Method of moments

The exact solution of the boundary value problem (Eqs. (2.1), (2.2), (2.3) and (2.4)) fulfils Eq. (2.1) identically. If one uses trial solution $H = H_p(z,t)$, Eq. (2.1) will be violated. Nevertheless, one can use $H_p(z,t)$ as an *approximate* solution, if it obeys 'conservation laws' for the moments M_n:

$$\dot{M}_n = \int_0^\infty z^n B\left[H_p(z,t)\right]\mathrm{d}z, \quad \text{where } M_n = \int_0^\infty z^n H_p(z,t)\mathrm{d}z. \tag{3.1}$$

Here, Eq. (2.1) was multiplied by z^n and integrated over z, and dot stands for time derivative. The number of differential equations in Eq. (3.1) should be equal to the number of time-dependent parameters characterizing $H_p(z,t)$. We consider two such parameters – surface temperature $T_s(t)$ and characteristic 'thermal length' $l(t)$ for the enthalpy distribution.

Therefore, we must use *two* first moments. Eqs. (2.4) and (3.1) yield:

$$\dot{M}_0 = -vH_s + J_s + I_s \equiv -v\left(L + H_{gs}\right) + I_s \qquad (3.2a)$$

$$\dot{M}_1 = -v\,M_0 + \int_{T_0}^{T_s} K(T)\,dT + I_s/\alpha \qquad (3.2b)$$

Here, $H_s \equiv H(T_s)$, $H_{gs} \equiv H_g(T_s)$. The equation for M_0 reflects the *time-dependent* energy balance. We set $H_p(z,t)$, in the form:

$$H_p(z,t) = \left[\left(H_s - lJ_s/D_s\right)e^{-\alpha z} - \left(\alpha l H_s - lJ_s/D_s\right)e^{-z/l}\right]/(1-\alpha l). \qquad (3.3)$$

This satisfies requirement $H_p(z=0,t) \equiv H_s(t)$ and boundary condition Eq. (2.4). The first term in Eq. (3.3) is related to absorption of radiation, while the second describes the changes in enthalpy distribution due to heat conduction. With $l=0$, Eq. (3.3) gives calorimetric solution. With $v = \text{const.}$, it coincides with the stationary ablation wave solution [6,7]. For the first two moments defined in Eq. (3.1), Eq. (3.3) yields:

$$M_0 = \left(l + \alpha^{-1}\right)H_s - \alpha^{-1} l J_s/D_s,$$
$$M_1 = \left(l^2 + l\alpha^{-1} + \alpha^{-2}\right)H_s - \left(l + \alpha^{-1}\right) \times \alpha^{-1} l J_s/D_s. \qquad (3.4)$$

When Eq. (3.4) is substituted into Eqs. (3.2a) and (3.2b), one obtains two ODE for T_s and l. All quantities should be written in terms of the surface temperature T_s. Namely, one should insert J_s and D_s from Eq. (2.4), I_s and v from Eqs. (2.2) and (2.3), and H_s from Eq. (2.1). Numerical computations were done with 'Mathematica' software package without resolving Eqs. (3.2a) and (3.2b) with respect to dT_s/dt and dl/dt.

The equation for the thickness of ablated material (coupled to Eqs. (3.2a) and (3.2b) via screening Eq. (2.2)) is given by (Eq. (2.4)):

$$\dot{h} = v = v_0 \exp(-T_a/T_s) \qquad (3.5)$$

Thus, the initial problem Eqs. (2.1), (2.2), (2.3) and (2.4) is reduced to three ODE for T_s, l, and h. The initial conditions are: $T_s(t=0) = T_0$, $l(t=0) = 0$, $h(t=0) = 0$. The solution of these equations coincides with analytical and numerical solutions of the initial problem Eqs. (2.1), (2.2), (2.3) and (2.4) within 10% accuracy.

4. Approximate analytical formulas for the generic case

Here we describe the general features of ablated depth vs. fluence curves. The deviations from the general trends will be discussed in subsequent sections. The temporal profile of the excimer laser pulse is approximated by the smooth function:

$$I(t) = I_0 \frac{t}{\tau}\exp\left[-\frac{t}{\tau}\right]. \qquad (4.1)$$

The laser fluence is given by $\phi = I_0\tau$ and pulse duration at the full widths at half maximum $t_{FWHM} \approx 2.446\tau$.

Fig. 1a gives an example of calculated ablation curve, which corresponds to the case which we call 'generic'. Heat penetration depth $\sim (D\tau)^{1/2}$, absorption length α^{-1} and ablated depth h are comparable for this case. The values of parameters are given in the figure caption. The ablation curve demonstrates remarkable simplicity, which holds even if some of parameters depend significantly on temperature. One can subdivide the ablation curve into three regions: Arrhenius tails, linear region and screening region.

4.1. Linear region and ablation threshold

At moderate fluences, or if screening can be neglected, the ablation curve in Fig. 1a is almost linear. Such a behavior is not self-evident with temperature-dependent material parameters and essential non-stationarity of the process. Fig. 1b demonstrates the sensitivity of the method. One can see the increase in the absorbed intensity and temperature at the initial stage of heating due to assumed linear increase in absorptivity $A(T_s)$, slowing down of the heating rate near the melting point, increase in heating rate due to smaller heat conduction at $T > T_m$, influence of ablation onset onto T_s, screening, etc. Thermal length l by no means stabilizes during the pulse. Neither does it correlate with the intensity I_s, as it would have been for the quasi-stationary ablation [9]. Nevertheless, $h(\phi)$ dependence *is* linear above $2 \div 3\phi_{th}$, as predicted by the quasi-stationary

consideration, though for somewhat different reasons – conservation of energy and sharp $v(T)$ dependence. Due to the latter, $v(t)$ changes much faster

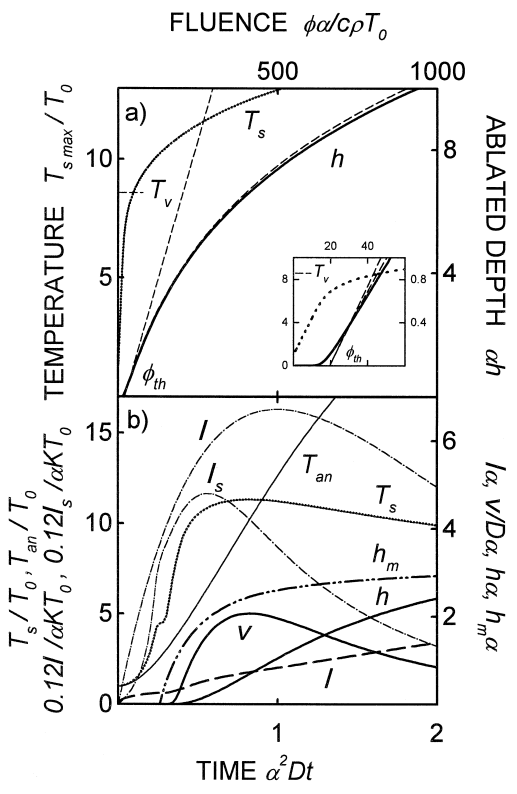

Fig. 1. (a) Ablated depth (solid curve) and maximal surface temperature (dotted curve) calculated from Eqs. (3.2a) and (3.2b) and Eq. (3.5) for laser pulse given by Eq. (4.1). Here, and in subsequent figures, thin dashed lines show linear approximations (Eq. (4.3) and Eq. (4.8)). Inset shows near threshold behavior. No melting. Dimensionless variables: Time $\alpha^2 Dt$, thermal length and ablated depth αl, αh, velocity $v/\alpha D$, temperature T_s/T_0, intensity $I/\alpha KT_0$, fluence $\phi\alpha/c\rho T_0$. Parameters satisfy the conditions: $A=1$, $\alpha^2 D\tau=1$, $v_0/D\alpha=10^3$, $L/\rho cT_0=20$, $T_a/T_0=70$, $H_g=H$, $\alpha_g=0.2\alpha$. They correspond, e.g., to $\tau=10$ ns, $D=10^{-2}$ cm^2/s, $\alpha=10^5$ cm^{-1}, $v_0=10^6$ cm/s, $T_a=21{,}000$ K $\equiv 1.81$ eV, $T_0=300$ K, $c=1$ J/gK, $\rho=1$ g/cm^3, $L=6$ kJ/cm^3 (strongly absorbing polymers). For these numbers, unit of time is 10 ns, of temperature 300 K, spatial unit 0.1 μm, and unit of fluence 3 mJ. (b) Time evolution of the surface temperature (dotted curve), ablated depth and ablation velocity (solid curves), thermal length (dashed curve) and molten depth (dash–double dot). Laser pulse and the laser intensity at the surface are shown by dash-dotted, temperature calculated analytically neglecting melting and ablation by thin solid curve. $\phi\alpha/c\rho T_0=370$. $\alpha_g=0.5\alpha$. Melting $T_m/T_0=4.5$, with the latent heat of fusion $H_m/\rho cT_0=3$ is introduced. Absorptivity increases linearly from $A(T_\infty)=0.2$ to $A(T_s\geq T_m)=$ const. $=0.9$. $K(T>T_m)=3K(T<T_m)$. Other parameters as in Fig. 1a.

than $T_s(t)$ (but not necessarily faster than $l(t)$!) (see Fig. 1b). Having this in mind, we integrate Eq. (3.2a) over time up to the moment when ablation and laser irradiation are finished and $v=0$, $J_s=0$. $L+H_{gs}$ is a slow function of time in comparison to v. We also assume constant absorptivity A to obtain analytical expressions. This, together with Eq. (3.4) for the M_0 yields:

$$A\phi = h\left(L+H_{gs}\right)+H_s\left(l+\alpha^{-1}\right). \qquad (4.2)$$

This reflects the energy conservation law. Absorbed fluence is spent on ablation (first term) and heating of the bulk (second term, which is the enthalpy content within the material M_0). The second term in Eq. (4.2) often does not change much at elevated fluences, and Eq. (4.2) yields linear $h(\phi)$ dependence:

$$h\approx B(\phi-\phi_{th}),\qquad B=\frac{A}{\left(L+H_{gs}\right)},$$

$$\phi_{th}=\frac{H_s\left(l+\alpha^{-1}\right)}{A}. \qquad (4.3)$$

At low fluences, the last term in r.h.s. of Eq. (4.2) dominates – laser mainly heats the material. In this region, T_s and H_s at the end of the pulse depend significantly on fluence. This is Arrhenius region. The transition to linear regime occurs when the two terms in Eq. (4.2) are comparable, i.e., laser energy splits about equally between the vaporization and the heating of material. To find typical surface temperature at this transition, T_v, we approximate h and l near the threshold as:

$$h\approx v(T_v)\,t_{FWHM},\qquad l\approx\left(\langle D(T_v)\rangle t_{FWHM}\right)^{1/2},$$

$$\text{with}\ \langle D(T_v)\rangle\equiv\left[\int_{T_0}^{T_v}K(T)\mathrm{d}T\right]/H(T_v) \qquad (4.4)$$

and equate both terms in r.h.s. of Eq. (4.2). This gives the equation for T_v:

$$v(T_v)\,t_{FWHM}\left[L+H_g(T_v)\right]$$
$$=H(T_v)\left[\left(\langle D(T_v)\rangle t_{FWHM}\right)^{1/2}+\alpha^{-1}\right]. \qquad (4.5)$$

When T_v is found, it should be substituted into temperature dependent quantities in Eq. (4.3) to give ϕ_{th} and the slope B of the ablation curve, as above threshold $T_{s\,max}$ changes slowly with increasing fluence (Fig. 1a).

In general, Eqs. (4.4) and (4.5) should be consid-

ered as a rule of thumb, deduced from the comparison with the numerical solution of Eqs. (3.2a) and (3.2b) with different temperature dependences in $K(T)$, $c(T)$ and $v(T)$. Linear dependence (Eq. (4.3)) is shown in Fig. 1a by the dashed line, together with T_v and ϕ_{th}. Several comments on this linear dependence are appropriate.

(i) Low temperature behavior of material parameters changes ϕ_{th}, but not the slope B of the ablation curve.

(ii) The slope B depends only on high temperature value of absorptivity and vaporization enthalpy. With $\phi \gg \phi_{th}$ ablation curves are quite insensitive to the temperature dependences of c and k.

(iii) ϕ_{th}, as defined by Eq. (4.3) is *not* the fluence 'spent on heating before the ablation starts'. It is what is ultimately wasted on heating, when the ablation is *finished*.

The last notion explains why good heat conductors obey linear law (Eq. (4.3)) *better*. The heat losses in this case are independent of ablation even at relatively high fluences.

4.2. Screening region

With the optical thickness of the plume in Eq. (2.2) proportional to the current value of h, we can multiply Eq. (3.2a) by $A^{-1}\exp(\alpha_g h)$ and rewrite it in a differential form:

$$d\phi = A^{-1}\left(L + H_{gs}\right)e^{\alpha_g h}dh + A^{-1}e^{\alpha_g h}dM_0 \qquad (4.6)$$

Now we integrate Eq. (4.6) with the argumentation similar to that which lead to Eq. (4.2). In the first term in r.h.s., all T_s-dependent quantities should be taken at T_v. The second term is more complicated. M_0 (the heating losses) changes only when ablation is present ($v \neq 0$) or radiation reaches the surface ($I_s \neq 0$) (see Eq. (3.2a)). This is fulfilled as long as $\alpha_g h < 1$, $\exp(\alpha_g h) \approx 1$. If screening does not significantly shorten the duration of laser intensity at the surface, we have for the last term in Eq. (4.6):

$$A^{-1}\int \exp(\alpha_g h)dM_0 \approx A^{-1}M_0(t_{FWHM}) \equiv \phi_{th} \qquad (4.7)$$

The last identity follows from Eqs. (3.4) and (4.3). With this approximation, after the integration, Eq. (4.6) yields for h:

$$h = \frac{1}{\alpha_g}\ln\left[1 + \alpha_g B(\phi - \phi_{th})\right] \qquad (4.8)$$

with B and ϕ_{th} given by Eq. (4.3) as before. The dependence (Eq. (4.8)) is shown in Fig. 1a by the dashed curve. Similar result was obtained in Ref. [9] from the quasi-stationary approximation. At moderate fluences with $\alpha_g h < 1$, Eq. (4.8) coincides with no screening result (Eq. (4.3)).

Linear and logarithmic approximations (Eqs. (4.3) and (4.8)) were verified by calculations with different temperature dependences in the specific heat, thermal conductivity, vaporization parameters and absorptivity. The Arrhenius tails at $\phi < \phi_{th}$, as well as ϕ_{th} itself are strongly affected by the temperature dependences in material parameters, evaporation rate characteristics, and pulse duration and shape.

The slope of the ablation curves B, to the contrary, is determined mainly by the latent heat of vaporization, high temperature absorptivity, and, in the case of screening, by the absorption coefficient of the plume α_g.

5. Deviations from the generic case

Here we study several cases when simple formulas (Eqs. (4.3), (4.4) and (4.5) or Eq. (4.8)) *do not* reflect peculiarities of the ablation process and/or etch curves.

5.1. Temporal profile of the laser pulse

Eqs. (4.3), (4.4) and (4.5) suggest that laser pulses of different shapes with the same t_{FWHM} result in identical ablation curves. In the region $\alpha^2 D t_{FWHM} \gg 1$, the solution of moments approximation reveals significant influence of the pulse shape onto ϕ_{th}, *not reflected* in Eqs. (4.3), (4.4) and (4.5). ϕ_{th} for the smooth pulse (Eq. (4.1)) can be about 30% higher than ϕ_{th} for the rectangular pulse with the same t_{FWHM}.

5.2. Small ablation enthalpy

Polymer ablation products may have much higher molecular weight than with inorganic materials [10]. As a result, ablation enthalpy *per gram* is significantly lower, and the specific heat and enthalpy of the condensed and the gas phase are almost equal. Besides, polymers easier undergo thermal destruction [3]. An extreme case with $L = 0$ and low $T_a/T_0 = 40$ is considered in Fig. 2a. As in the generic case, the curves have pronounced threshold associated with significant increase in $v(T_s)$. At the same time, $h(\phi)$ dependence has an inflection point at low fluences, and is slower than linear at high fluences. This decrease in slope is *unrelated to screening*. Its parameters are determined by the $v(T_s)$ and $H_g(T_s)$ dependences.

5.3. Temperature dependent shielding

At high fluences, the amount of ablated material depends mainly on the plume properties. We model a sharp increase in α_g with temperature due to ionization [7,11] by the model dependence:

$$\alpha_g/\alpha = C\exp(-T_\alpha/T_s) \qquad (5.1)$$

T_α is close to ionization potential in Kelvin. Fig. 4b demonstrates, that despite sharp dependence (Eq. (5.1)), the ablation curve resembles the generic case depicted in Fig. 1a. At low fluences, it follows linear approximation more closely. At high fluences, it is slower than logarithmic. The transition to the screening regime occurs at fluences, where $\alpha_g(T_{s\,max})h(T_{s\,max}) \approx 1$, and at higher fluences, h is rather insensitive to the details of $\alpha_g(T_s)$ dependence.

5.4. Ablation of weakly-absorbing materials

Simple approximations (Eqs. (4.3), (4.4) and (4.5)) fail if $\alpha^2 D\tau < 1$. Here, modelling reveals four stages of heating and ablation (Fig. 3a). Initially, both the surface movement and the heat conduction may be ignored. Then, recession velocity becomes significant, which slows down the heating of the surface. Subsurface heated layer is formed at this stage.

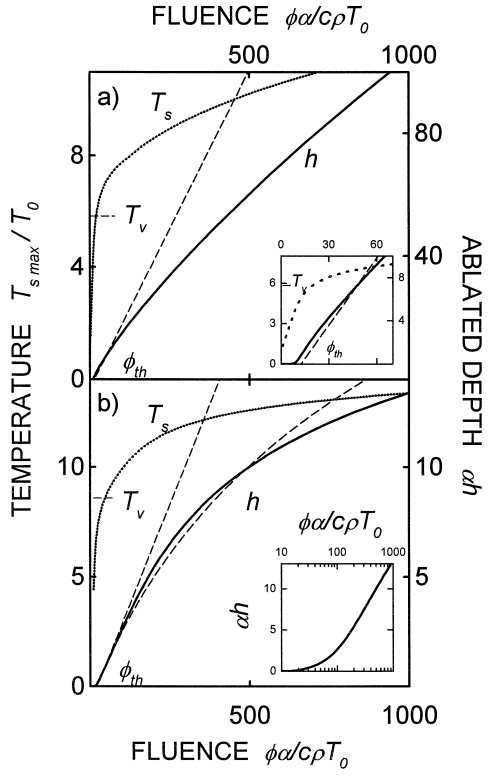

Fig. 2. (a) Easily decomposing material with $T_a/T_0 = 40$, $L/\rho cT_0 = 0$. No screening, other parameters as in Fig. 1a. Inset shows near threshold behavior. (b) Temperature dependent screening (Eq. (5.1)) with $T_\alpha = 130T_0$, $C = 10^4$ ($\alpha_g \approx \alpha$ with $T_s/T_0 \approx 14.1$). Logarithmic approximation (Eq. (4.8)) (thin dashed curve) is calculated with $\alpha_g/\alpha = 0.1$. Inset: h vs. log ϕ.

Then, the ablation front catches up with the heated layer, which is reflected by the decrease in $l(t)$. When the ablation velocity reaches certain value, $T_s(t)$ and $v(t)$ sharply increase. This corresponds to the ablation of the heated subsurface layer, which exists due to the positive temperature gradient at the surface (Eq. (2.4)). Finally, after the end of the pulse, the surface slowly cools down by heat conduction. Significant amount of material is ablated at this stage. For the numbers employed in Fig. 3, ablation ceases at $\alpha^2 Dt \approx 1$–10.

The fluence for the 'second threshold' – i.e., the

sharp increase in T_s and v can be estimated from the time to heat the layer of thickness $\sim 1/\alpha$ [6]:

$$t_2 \approx 1/\alpha v \approx (L + H_{gs})/\alpha AI$$
$$\Rightarrow \phi_2 \approx It_2 \approx (L + H_{gs})/\alpha A. \quad (5.2)$$

The thickness $h(\phi_2) \approx 1/\alpha$ is ablated with this fluence. With constant parameters, second threshold is weakly-reflected in the ablation curve (Fig. 3b) because the ablation of subsurface layer may occur also *after* the pulse. With $\phi < \phi_2$, when the pulse is finished, l and the overheated layer are larger, cooling is slower, and more material is ablated after the pulse. The change in ablation curves may be more significant if, e.g., absorptivity A depends on T_s. In this case, the slope of the ablation curve at ϕ_2 may change significantly according to Eq. (4.3), as $T_{s\,max}$ may increase almost twice in a narrow fluence interval near ϕ_2 (Fig. 3b).

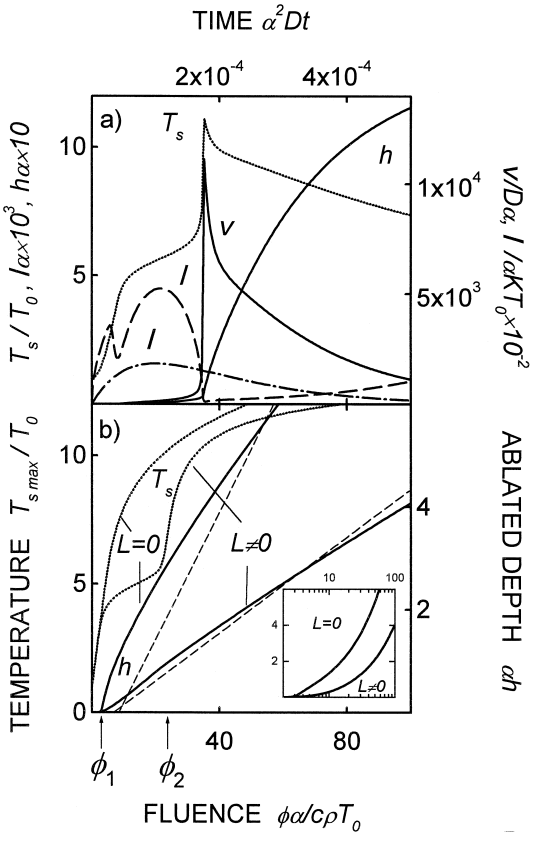

Fig. 3. (a) Weakly-absorbing material. Time evolution of the surface temperature (dotted curve), ablated depth and ablation velocity (solid curves), and thermal length (dashed curve). Temporal shape of laser pulse is shown by dash-dotted curve. $\phi\alpha/c\rho T_0 = 50$. $A = 1$, $\alpha^2 D\tau = 10^{-4}$, $v_0/D\alpha = 10^6$, $L/\rho c T_0 = 15$, $T_a/T_0 = 50$, $H_g = H_s$, $\alpha_g = 0$. This corresponds, e.g., to $\tau = 10$ ns, $D = 10^{-3}$ cm^2/s, $\alpha = 3.16\times10^3$ cm^{-1}, $v_0 = 3.16\times10^6$ cm/s, $T_a = 15{,}000$ K $\equiv 1.29$ eV, $T_0 = 300$ K, $c = 1$ J/gK, $\rho = 1$ g/cm^3, $L = 4.5$ kJ/cm^3. With these numbers, unit of time is 100 μs, of temperature 300 K, spatial unit 3.16 μm, and unit of fluence 95 mJ. (b) Ablation curves for $L/\rho c T_0 = 15$, ($\phi_{th}\alpha/c\rho T_0 = 6.58$, $T_v/T_0 = 7.48$) and $L = 0$. Second threshold ϕ_2 (Eq.(5.2)), and threshold ϕ_1 calculated from Eq. (5.3) are shown for $L \neq 0$.

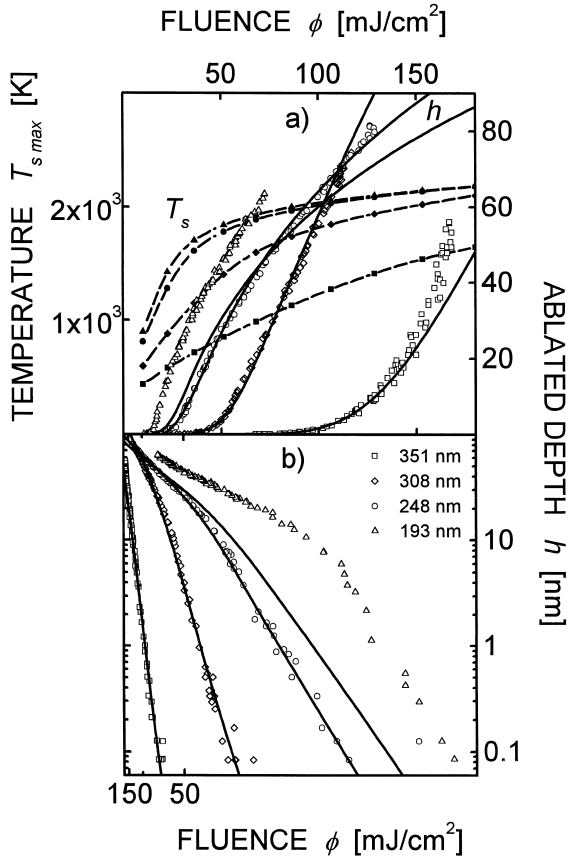

Fig. 4. Modelling of the single-pulse ablation of PI. (a) Ablation curves and calculated $T_{s\,max}$. (b) Arrhenius plot of ablation curves. $\tau = 6.13$ ns ($t_{FWHM} = 15$ ns), $v_0 = 3\times10^6$ cm/s, $T_a = 17{,}500$ K, $T_0 = 300$ K, $c = 2.55 - 1.59\times\exp((300-T)/460)$ J/gK, $c_g = 2.55$ J/gK, $K = 1.55\times10^{-3}\times(T/300)^{0.28}$ W/cmK, $\rho = 1.42$ g/cm^3, $L/\rho = 0.5$ kJ/g, $\alpha_g = 0.45\alpha$. $\lambda = 193$ nm (triangles): $A = 0.93$, $\alpha = 4.25\times10^5$ cm^{-1}; $\lambda = 248$ nm (circles): $A = 0.88$, $\alpha = 3.1\times10^5$ cm^{-1}; $\lambda = 308$ nm (diamonds): $A = 0.89$, $\alpha = 10^5$ cm^{-1}; $\lambda = 351$ nm (squares): $A = 0.9$, $\alpha = 0.32\times10^5$ cm^{-1}.

Fig. 3b (dashed curves) shows, that Eq. (4.3) overestimates ϕ_{th} and T_v because the ablation takes place mainly *after* the pulse, and it is erroneous to use t_{FWHM} in Eq. (4.4). Neglecting the influence of ablation on cooling, one can estimate the fluence ϕ_1 at the 'first threshold' as:

$$\left[L + H_g(T_1)\right] \frac{2\upsilon_0}{\alpha^2 D} \left[\frac{T_1}{T_a}\right]^2 \exp\left[-\frac{T_a}{T_1}\right] \approx A\phi_1/2,$$

$$T_1 = T_0 + \frac{A\alpha\phi_1}{c\rho} \qquad (5.3)$$

Here, T_1 is the temperature rise just after the end of the laser pulse. Arrhenius dependence in Eq. (5.3) makes ϕ_1 about proportional to $c\rho T_a/A\alpha$ and less sensitive to other parameters.

The second threshold is due to vaporization enthalpy L (compare with the $T_s(\phi)$ curve for $L = 0$), as with $L = 0$ gradient (Eq. (2.4)) is zero. For $L = 0$, approximations (Eqs. (4.3), (4.4) and (4.5)) work even worse than in Fig. 2a. The $h(\phi)$ dependence is faster than logarithmic but slower than linear as observed in many experiments [2,10].

Fig. 4 shows the modelling of the single-pulse ablation of Polyimide (Kapton™ H) [12]. The fit of the region $\phi < \phi_{th}$ with temperature dependent parameters from [13,14] for 248, 308 and 351 nm yields a *single* activation energy ($T_a = 17500$ K ≡ 1.51 eV ≡ 146 kJ/mol), close to that reported for the thermal degradation of PI [3]. The ablation curves at *higher fluences* are fitted by varying L and plume attenuation coefficient α_g. Here, the fit is ambiguous, since increase in both of them decreases the slope of the ablation curves. Data at 193 nm demonstrate significant deviations. This suggests either quite different mechanisms, or significant change in material properties.

6. Conclusions

We applied the method of non-stationary averaging to study the influence of different factors onto ablation curves within the frame of *surface thermal evaporation* model. Due to its speed and flexibility, the method provides powerful tool for the fast analysis of the experimental data. The consideration of time-dependent thermal length gives additional insight into the ablation dynamics.

The ablation curves may be subdivided into three regions of fluence.

(i) Arrhenius region, where laser energy mainly goes to the heating of the material;

(ii) linear region, where the ablated depth increases linearly with fluence due to the overall energy balance and;

(iii) screening region, where shielding of radiation by the ablation products plays an important role.

Analytical formulas for the threshold fluence ϕ_{th}, and $h(\phi)$ dependences at $\phi > \phi_{th}$ are discussed.

Small vaporization enthalpy results in a sub-linear but faster than logarithmic $h(\phi)$ dependence. This may explain the increase in slope in $\log(h)$ vs. ϕ dependences observed in experiments.

With weakly-absorbing materials, ablation may proceed with or without the ablation of the heated subsurface layer. The latter occurs at higher fluences and reveals significantly higher ablation temperatures, but is only weakly-reflected in the ablation curves.

As an example, single-pulse ablation of polyimide is analyzed with the method of moments.

Acknowledgements

The authors are grateful to the Russian Basic Research Foundation, INTAS (grant 94-902), and the 'Fonds zur Förderung der wissenschaftlichen Forschung in Österreich' for financial support.

References

[1] D. Bäuerle, Laser Processing and Chemistry, 2nd ed., Springer, Berlin, 1996.
[2] R. Srinivasan, Interaction of laser radiation with organic polymers, in: J.C. Miller (Ed.), Springer Series in Materials Science, 28, Springer, 1994, p. 107.
[3] W.W. Wright, in: N. Grassie (Ed.), Developments in Polymer Degradation-3, Appl. Sci. Publisher, London, 1981.
[4] B. Luk'yanchuk, N. Bityurin, M. Himmelbauer, N. Arnold, Nucl. Instr. Meth. B 122 (1997) 347.
[5] D. Zwillinger, Handbook of Differential Equations, Academic Press, Boston, 1989.

[6] S.I. Anisimov, V.A. Khokhlov, Instabilities in Laser–Matter Interaction, CRC Press, Boca Raton, 1995.
[7] S.I. Anisimov, Ya.A. Imas, G.S. Romanov, Yu.V. Khodyko, Action of High-Power Radiation on Metals, National Technical Information Service, Springfield, VA, 1971.
[8] X. Mao, R.E. Russo, Appl. Phys. A 64 (1997) 1.
[9] V.N. Tokarev, J.G. Lunney, W. Marine, M. Sentis, J. Appl. Phys. 78 (2) (1995) 1241.
[10] R. Srinivasan, B. Braren, Chem. Rev. 89 (1989) 1303.
[11] Y.B. Zeldovich, Yu.P. Raizer, Physics of Shock Waves and High-Temperature Hydrodynamic Phenomena, Academic Press, London, 1966.
[12] S. Küper, J. Brannon, K. Brannon, Appl. Phys. A 56 (1993) 43.
[13] E.T. Arakawa, M.W. Williams, J.C. Ashley, L.R. Painter, J. Appl. Phys. 52 (1981) 3579.
[14] J.H. Brannon, J.R. Lankard, A.I. Baise, F. Burns, J. Kaufman, J. Appl. Phys. 58 (5) (1985) 2036.